Stoichiometry-Dependent Formation of Quantum Dot−Antibody Bioconjugates: A Complementary Atomic Force Microscopy and Agarose Gel Electrophoresis Study

Barrett J. Nehilla,[†,‡] Tania Q. Vu,[§] and Tejal A. Desai*[,†]

Department of Biomedical Engineering, 44 Cummington Street, Whitaker Labs Room 701, Boston University, Boston, Massachusetts 02215, Department of Pharmacology and Experimental Therapeutics, 715 Albany Street, Room L-603, Boston University, Boston, Massachusetts 02218, and Department of Biomedical Engineering, OGI School of Science & Engineering, Oregon Health & Science University, 20000 NW Walker Road, Beaverton, Oregon 97006

Received: May 18, 2005; In Final Form: September 13, 2005

The unique advantages of quantum dot (QD) bioconjugates have motivated their application in biological assays. However, physical characterization of bioconjugated QDs after surface modification has often been overlooked. Here, biotinylated antibodies (biotin−IgG) were attached to commercial streptavidin-conjugated quantum dots (strep−QDs) at different stoichiometric ratios, and these QD bioconjugates were characterized with atomic force microscopy and discontinuous sodium dodecyl sulfate agarose gel electrophoresis (SDS-AGE). The results from these complementary analytical techniques showed that the molar ratio determined the relative sizes, molecular weights and morphologies of the QD bioconjugates. Additionally, the novel discontinuous SDS-AGE analysis confirmed specific binding between biotin−IgG and strep−QDs. Researchers who design QD bioconjugates for cell-based assays should consider stoichiometry-dependent differences in the physical properties of their QD bioconjugates.

Introduction

Quantum dots (QDs) have recently entered the realm of biology because of their myriad advantages as biological probes: nanoscale size similar to proteins, bright fluorescence, versatility in surface modification, broad excitation spectra for multicolor imaging, and robust, narrow-band emission.[1] Stable, water-soluble QDs with defined surface chemistries permit surface modification with various biomolecules (e.g., peptides, oligonucleotides, proteins) for in vitro and in vivo targeting, labeling, and imaging applications.[2−5] Knowledge of QD surface chemistry is imperative to understanding the interface and behavior between the inorganic semiconductor core and shell and the biological system. Still, many researchers utilize water-soluble, bioconjugated QDs in biological assays without characterizing the entire bioconjugate.[2,6−9] Applying QD bioconjugates to biological systems without characterization is premature, and it complicates experimental interpretations. We controlled QD bioconjugate formation in a stoichiometry-dependent manner by exploiting streptavidin−biotin chemistry. Streptavidin−biotin binding has been used extensively for surface conjugation of proteins, with expansive biotechnological and diagnostic applications.[10−12] Commercial streptavidin-conjugated QDs (strep−QDs) are exciting nanoscale tools because they combine QD advantages with the high affinity and simplicity of streptavidin−biotin based conjugations and assays. The sensitivity and specificity of in vitro fluorescence assays may be significantly enhanced with antibody−QD immunoconjugates, so we investigated QDs modified with a model biotinylated IgG antibody. Specifically, we attached biotin−IgG molecules to commercial, strep−QDs at different molar ratios and characterized the sizes, morphologies, molecular weights, and specific binding of these QD bioconjugates using complementary analytical techniques from materials science, atomic force microscopy (AFM), and molecular biology, discontinuous sodium dodecyl sulfate agarose gel electrophoresis, (SDS-AGE).

Tapping-mode AFM is versatile for examining the surface nanostructure of both inorganic and biological samples, with negligible surface damage or "dragging" compared to contact mode. It provides qualitative and quantitative information with Angstrom-level resolution[13] regarding the diameter, height, morphology, and organization of surface-adsorbed nanoparticles. Topography AFM has been utilized for size characterization of QDs after surface modification and peptide immobilization.[14,15] Here, topography AFM and subsequent cross-section height analysis were used to quantify QD bioconjugate heights, while phase AFM elucidated morphology characteristics. In phase AFM, the phase lag between the excitation signal and cantilever response measures the topography, friction, elasticity, stiffness, and other material surface properties.[16−19] Despite these advantages, AFM phase analysis of nanoparticles has only recently been published.[20,21] In this work, phase imaging afforded higher resolution through improved contrast of QD bioconjugate shapes, allowed morphology visualization and supplemented size information from topography AFM. Combining AFM topography and phase modalities allowed an initial assessment of the sizes and morphologies of strep−QDs and QD bioconjugates.

AGE is typically used to study nucleic acid migration, perform electrophoretic mobility shift assays, and separate high molecular weight species. Polyacrylamide typically affords better protein resolution, but agarose is appropriate here because commercial strep−QDs are much heavier (∼500 kDa) than most

* To whom correspondence should be addressed. E-mail: tdesai@bu.edu. Phone: 617-358-2832. Fax: 617-358-2835.

[†] Department of Biomedical Engineering, Boston University.

[‡] Department of Pharmacology and Experimental Therapeutics, Boston University.

[§] Department of Biomedical Engineering, Oregon Health & Science University.

10.1021/jp052613+ CCC: $30.25
Published on Web 10/19/2005

biomolecules.[22] Nucleic acid modified gold nanoparticles have been analyzed with continuous AGE,[23−25] but electrophoretic characterization of peptide and oligonucleotide-modified QDs only recently entered the literature.[14,26,27] In those studies, continuous AGE elucidated the sizes and surface properties of lab-synthesized QDs[14,27] or the binding of biotinylated oligonucleotides to commercial strep−QDs.[26] We believed the resolution in published electrophoresis studies was suboptimal, so we developed a unique, discontinuous SDS-AGE system with much improved resolution over continuous SDS-AGE and SDS polyacrylamide gel electrophoresis (SDS-PAGE). To our knowledge, this is the first report of discontinuous SDS-AGE employed to characterize protein-modified commercial QD bioconjugates. Our SDS-AGE experiments elucidated the relative sizes and molecular weights of strep−QDs and QD bioconjugates, and the migration patterns confirmed specific antibody binding to strep−QDs. Furthermore, the size and morphology conclusions drawn from topography and phase AFM analysis were corroborated by discontinuous SDS-AGE. Only by integrating AFM and electrophoresis could we completely characterize the stoichiometry-dependent size, molecular weight, and morphology differences between the QD bioconjugates and confirm specific biotin−IgG:streptavidin binding in the QD bioconjugates.

Experimental Details

Chemicals and Reagents. Biotin, (3-aminopropyl)triethoxysilane (APTES), and biotinylated rabbit anti-mouse IgG (biotin−IgG) were purchased from Sigma (St. Louis, MO). Quantum dots with 655-nm wavelength emission consisted of a CdSe/ZnS core−shell structure surrounded by a proprietary polymeric coating and conjugated streptavidin molecules (Quantum Dots, Corp., Hayward, CA; part #1012-1). SDS was from Pierce Biotechnology (Rockford, IL). Certified Low Range Ultra Agarose powder and bromophenol blue (BMB) were acquired from Bio-Rad (Hercules, CA). Tris(hydroxymethyl)aminomethane (Tris) and glycine (Gly) were from EMD Biosciences, Inc. (San Diego, CA). All QD or QD bioconjugate solutions were diluted in PBS, pH 7.2, from BupH Phosphate Buffered Saline Packs (Pierce).

Mica Silanization. Muscovite mica disks, 9.9 mm diameter (SPI Supplies, West Chester, PA), were cleaved with a scalpel and immediately silanized. The freshly cleaved mica pieces were placed in a vacuum oven (Fisher Scientific Isotemp, Pittsburgh, PA) beside a glass dish with APTES (∼0.6 mL per mica disk). Mica surfaces were exposed to 23 mm Hg vacuum, heated for 195 min at 180°C, and allowed to sit in silane vapor at atmospheric pressure for 15 min. After silanization, mica surfaces were used immediately or stored in a vacuum.

Quantum Dot and Bioconjugate Adsorption. Strep−QDs or QD bioconjugates (different biotin−IgG:strep−QD molar ratios) were prepared in PBS and adsorbed onto silanized mica surfaces using a simple passive adsorption scheme. An 8-μL solution of strep−QDs or QD bioconjugates was pipetted on the mica and allowed to adsorb for 20 min. Afterward, the mica was rinsed gently with 10 mL DIH_2O, dried in a N_2 stream, and analyzed immediately. Solutions were made immediately before adsorption of strep−QDs or QD bioconjugates to mica surfaces: strep−QDs (2 nM), biotin−QDs (750 nM biotin and 8 nM strep−QDs), 100:1 QD bioconjugates (1 μM biotin−IgG and 10 nM strep−QDs), 1:1 QD bioconjugates (15 nM biotin−IgG and 15 nM strep−QDs), free biotin−IgG (500 nM), and biotin-blocked strep−QDs (16 nM strep−QDs and 750 nM biotin, followed by 16 nM biotin−IgG).

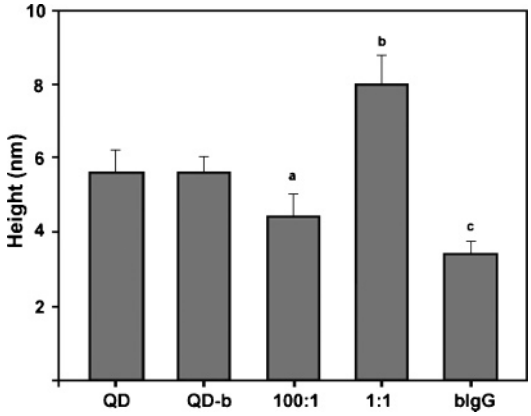

Figure 1. Topography AFM height analysis showed that the biotin−IgG:strep−QD molar ratio determined QD bioconjugate heights. Strep−QD and QD bioconjugate mean heights for individual scans ($N \geq 10$) were calculated from at least three different surfaces. The following labels were used: QD (strep−QD), QD−b (biotin−QD), 100:1 and 1:1 (biotin−IgG:strep−QD molar ratio), bIgG (biotin IgG). Quantitative height measurements for these surfaces were (group mean ± SEM, in nm): 5.64 ± 0.127, 5.64 ± 0.164, 4.48 ± 0.126, 8.00 ± 0.200, and 3.47 ± 0.092, respectively. Error bars are standard deviations. One-way ANOVA with Holm−Sidak post-hoc analysis was performed to compare multiple groups ($p < 0.01$ for significance). (a) Statistically different from QD, QD-b, 1:1, and bIgG. (b) Statistically different from QD, QD−b, 100:1, and bIgG. (c) Statistically different from QD, QD−b, 100:1, 1:1.

AFM. A Quesant Q-Scope 250 (Quesant Instruments, Corp., Agoura Hills, CA) was operated in tapping mode. Standard silicon cantilevers (Quesant) with a force constant ∼40 N/m, resonant frequency ∼137 kHz, and radius of curvature <10 nm were used. Topography and phase images were simultaneously collected at a scan rate of 2 Hz under ambient laboratory conditions. The heights of surface features were measured from cross-section height profiles extracted via Q-Analysis software (Quesant), and the mean height for each surface scan was calculated for subsequent statistical analysis. All significance tests were performed with SigmaStat.

Discontinuous SDS-AGE. Gels were hand cast with agarose (Bio-Rad) in the appropriate buffers. In detail, agarose for the resolving gel was briefly boiled in buffer, cooled to ∼55 °C, and poured into a standard 7-cm^2 gel tray (Bio-Rad). After setting, 2 cm of the resolving gel was removed with a scalpel. Agarose for the stacking gel was also boiled, cooled, and poured to set so that the sample wells were ∼1 cm above the resolving gel (Figure 3). Gels were equilibrated overnight at 4 °C. AGE was performed with the Mini Sub-Cell Agarose Gel Electrophoresis System (Bio-Rad), in which gels were immersed horizontally for electrophoresis. Samples were diluted in sample buffer (62.5 mM Tris, 2% SDS, 10% glycerol, 0.2% BMB) for 15 min, loaded into the gels, and run for 90 min at 90 V. The final strep−QD concentration in each well was 12.5 nM. Tank buffer was 250 mM Gly, 192 mM Tris with 0.1% SDS (pH 8.3), resolving gel buffer was 375 mM Tris with 0.1% SDS (pH 8.8) for 1.75% gels, and stacking gel buffer was 125 mM Tris with 0.1% SDS (pH 6.8) for 0.5% gels. For QD visualization, the gel was placed on a UV transilluminator (FotoPrepI, Fotodyne, Inc., Hartland, WI), and its image was captured with the Alphaimager camera-software package (AlphaInnotech, San Leandro, CA).

Results and Discussion

The properties of strep−QDs and QD bioconjugates were first characterized with topography and phase AFM because AFM

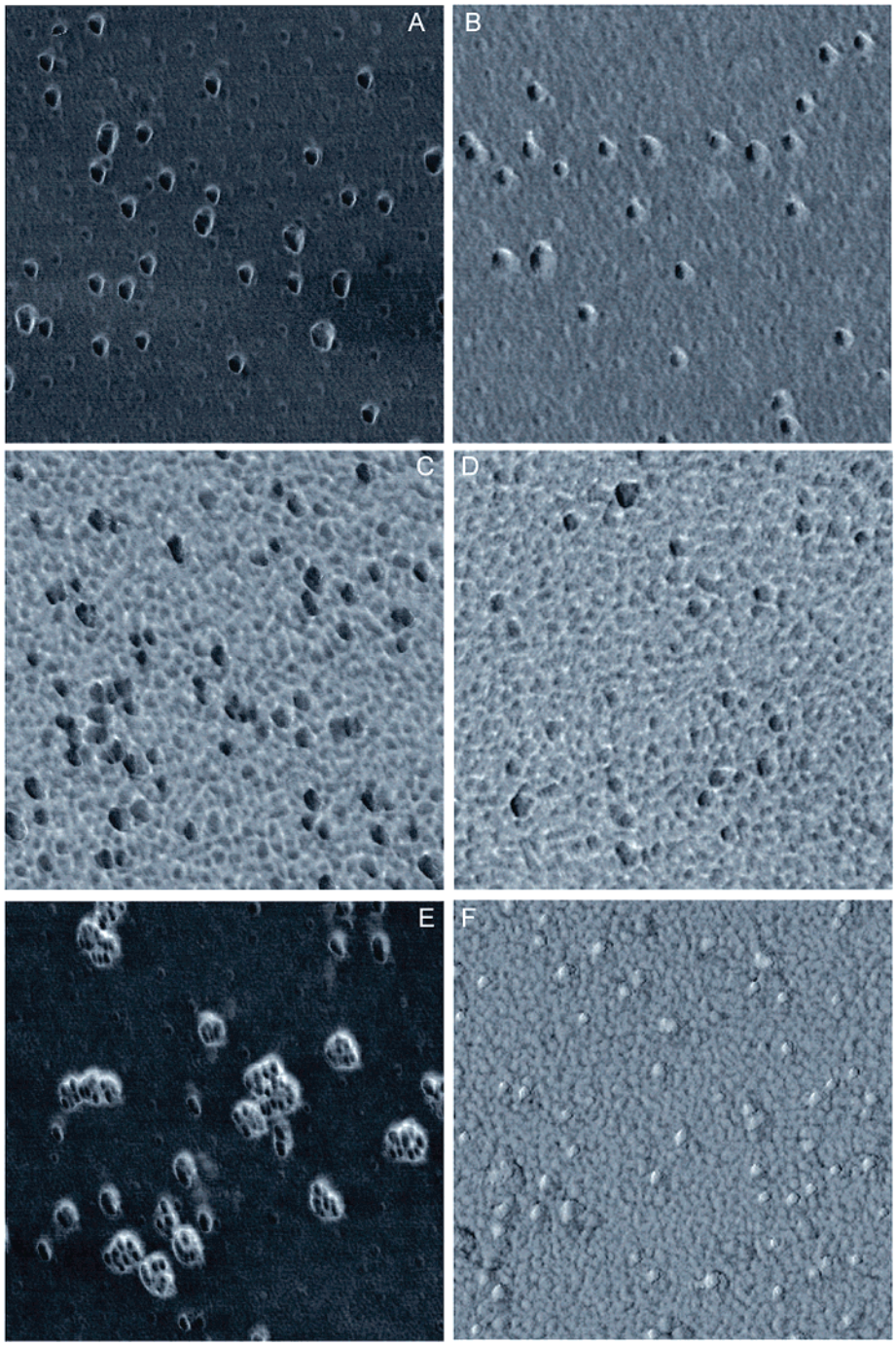

Figure 2. AFM phase images of strep−QDs and QD bioconjugates allowed visualization of morphology characteristics. Discrete strep−QDs (A, 2 nM) and biotin−QDs (B, 8 nM strep−QD:750 nM biotin) were well defined with similar size and morphology. The 100:1 bioconjugate (C, 1 μM biotin−IgG:10 nM strep−QD) and biotin−IgG (D, 500 nM) surfaces were similar, with a closely packed surface layer and larger indistinguishable features. Individual strep−QDs were easily discerned in networks of 1:1 bioconjugates (E, 15 nM biotin−IgG:15 nM strep−QD), and this phenomenon was prevented by blocking binding sites with biotin before biotin−IgG incubation (F, 16 nM strep−QD:750 nM biotin, followed by 16 nM biotin−IgG). All images are 1 μm^2.

is a powerful nanocharacterization tool. Familiarity with sample−substrate interactions is necessary to exploit the high-resolution capability of AFM for biomolecular imaging.[13] Atomically flat mica surfaces are ideal substrates for AFM imaging, but strep−QDs did not bind to its negatively charged surface. This was probably due to streptavidin's low isoelectric point and negative charge at physiological pH. Thus, mica surfaces were treated with APTES to enhance adsorption because organosilanes such as APTES have promoted both biomolecule and QD binding to silicon substrates.[28,29] Strep−QD binding to APTES-treated mica was significantly enhanced (data not shown), so these treated surfaces were used for subsequent AFM analysis.

Strep−QDs and QD bioconjugates were analyzed with topography AFM to quantify stoichiometry-dependent size changes. As expected, height differences depended on the biotin−IgG:strep−QD molar ratio (Figure 1). Biotinylating the strep−QDs did not alter the heights (strep−QDs $\sim$ 5.6 nm, biotin−QDs $\sim$ 5.6 nm) because biotin is likely buried in its binding site.[30] The strep−QD height reported here agreed with published data[20] even though these commercial strep−QDs have

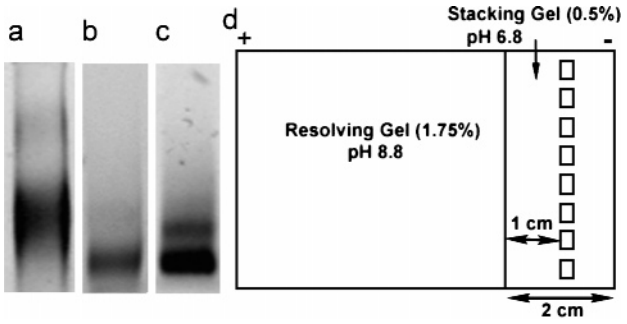

Figure 3. A unique discontinuous SDS-AGE system was developed to characterize relative strep−QD and QD bioconjugate sizes and molecular weights. Resolution of 12.5 nM strep−QDs with discontinuous SDS-AGE (panel c) was considerably better than continuous 4% SDS-PAGE (panel a) and continuous 1.75% SDS-AGE (panel b). Schematic of the stacking and resolving agarose gels of this discontinuous SDS-AGE system (panel d).

putative diameters of ∼22 nm, as measured by size-exclusion high-performance liquid chromatography (SE-HPLC).[22] In other work, ambient AFM size measurements of QDs were also much lower than sizes measured with SE-HPLC,[14] so the current height discrepancy is not unprecedented. Additionally, tip−sample interactions may have flattened streptavidin molecules on strep−QD surfaces[30] or affected the tip's resonance frequency,[31] both of which could artificially lower AFM height measurements. The 1:1 bioconjugates were significantly higher (∼8.0 nm) than strep−QDs but the 100:1 bioconjugate heights were significantly smaller (∼4.5 nm) than strep−QDs. We expected both 100:1 and 1:1 QD bioconjugates to be larger than strep−QDs, so this result warranted further investigation. Free biotin−IgG was significantly smaller (∼3.5 nm) than both strep−QDs and 100:1 bioconjugates, although this height was larger than previous tapping-mode AFM reports of mica-adsorbed IgG molecules (∼2 nm).[31−33] The ∼1.5 nm higher measurements reported here may have been due to the deposition of biotin−IgG molecules on top of a biotin−IgG surface monolayer. Height quantification from AFM topography images showed that biotin−IgG molecules were the smallest features, followed by 100:1 bioconjugates, strep−QDs, and biotin−QDs and 1:1 bioconjugates.

Although AFM topography analysis established preliminary quantitative height differences between strep−QDs and QD bioconjugates, it was complicated by the surprisingly small 100:1 bioconjugate heights. To improve AFM analysis, AFM phase imaging was performed to enhance the contrast of surface details, to corroborate height data from topography scans, and most importantly, to visualize strep−QD and QD bioconjugate morphologies. AFM phase images of strep−QDs and QD bioconjugates showed pronounced features (representative images in Figure 2). As expected from AFM height analysis, strep−QDs and biotin−QDs exhibited similar sizes and shapes (panels A and B of Figure 2). Most of these strep−QDs and biotin−QDs were single particles, although larger particles (i.e., dimers) were also visible. The 1:1 bioconjugates were much larger, and phase imaging resolved individual strep−QDs in biotin−IgG:QD cross-linked networks (panel E of Figure 2). Completely blocking streptavidin binding sites with excess biotin before biotin−IgG incubation prevented network formation (panel F of Figure 2), which suggested that 1:1 bioconjugate networks were assembled through specific streptavidin−biotin binding. The 100:1 and biotin−IgG surfaces were comprised of closely packed biotin−IgG surface layers with discrete but indistinguishable larger features (panels C and D of Figure 2). These large features may have been 100:1 bioconjugates embedded within the excess biotin−IgG monolayer (panel C of Figure 2) and individual IgG molecules above the biotin−IgG surface monolayer (panel D of Figure 2). This interpretation intimated that the full height of 100:1 bioconjugates may have been masked by the excess biotin−IgG surface layer or that IgG molecules above the monolayer were mistakenly measured as 100:1 bioconjugates. Both possibilities could explain the surprisingly low 100:1 QD bioconjugate height. Phase AFM could not distinguish 100:1 QD bioconjugates from biotin−IgG molecules because the semiconductor QD cores were coated with soft proteins. Therefore, further investigation of these QD bioconjugates with discontinuous SDS-AGE was necessary. Although AFM phase analysis did not confirm 100:1 bioconjugate formation, it strengthened AFM height conclusions for strep−QDs, biotin−QDs, and 1:1 bioconjugates and showed specific streptavidin:biotin−IgG mediated networking in 1:1 bioconjugates. Most importantly, phase AFM allowed visualization of QD bioconjugate morphologies that was not possible with topography AFM.

AFM has been employed to characterize the size of water-soluble QDs.[15,34] In addition, AFM has confirmed peptide conjugation to lab-synthesized QDs based on nanoscale size differences.[14] However, this is the first study to combine quantitative AFM height analysis with phase imaging of commercial strep−QDs in order to show stoichiometry-dependent differences in QD bioconjugate sizes and morphologies. These results showed that AFM established preliminary height and morphology characteristics of strep−QDs and QD bioconjugates. However, this technique was time-consuming and incomplete as a stand-alone method due to indeterminate specific conjugation in 100:1 QD bioconjugates.

Discontinuous SDS-AGE was performed to substantiate conclusions drawn from AFM data, determine relative sizes and molecular weights of QD bioconjugates, and further investigate specific biotin−IgG:streptavidin surface binding. In our initial electrophoresis studies, strep−QDs and QD bioconjugates were poorly resolved in continuous (single) agarose and polyacrylamide gels without SDS. To improve resolution, a stacking agarose gel was cast above the resolving gel and SDS was added to the buffers to mimic discontinuous SDS-PAGE,[35] a modification of the work of Raines.[36] Band resolution was enhanced with discontinuous SDS electrophoresis because SDS imparted a uniform mass:charge density to the samples, and the samples were condensed into a thin band between glycine and chloride ion fronts at the stacking/resolving gel interface.[37] In fact, our discontinuous SDS-AGE system exhibited markedly better resolution and tighter strep−QD bands than continuous 1.75% SDS-AGE and continuous 4% SDS-PAGE (Figure 3). The presence of distinct strep−QD bands here is in contrast with another electrophoresis study that reported one diffuse strep−QD band.[26] Banding was not due to SDS-mediated disruption of strep−QD surfaces because streptavidin molecules, streptavidin−biotin complexes, and the covalent bonds between streptavidin and the QD surface were stable in SDS.[12,38] Therefore, the multiple strep−QD bands resolved here were evidence of the much-improved resolution that our discontinuous SDS-AGE system offers. Discontinuous SDS-AGE was thus used to investigate relative size and molecular weight changes in addition to specific binding after antibody conjugation of commercial strep−QDs.

After running gels loaded with strep−QDs (lane 1) and QD bioconjugates (lanes 2−6), differences in relative molecular weights were apparent (Figure 4, panel A). In lane 1 (strep−QDs), there was a prominent band and a lighter band, which

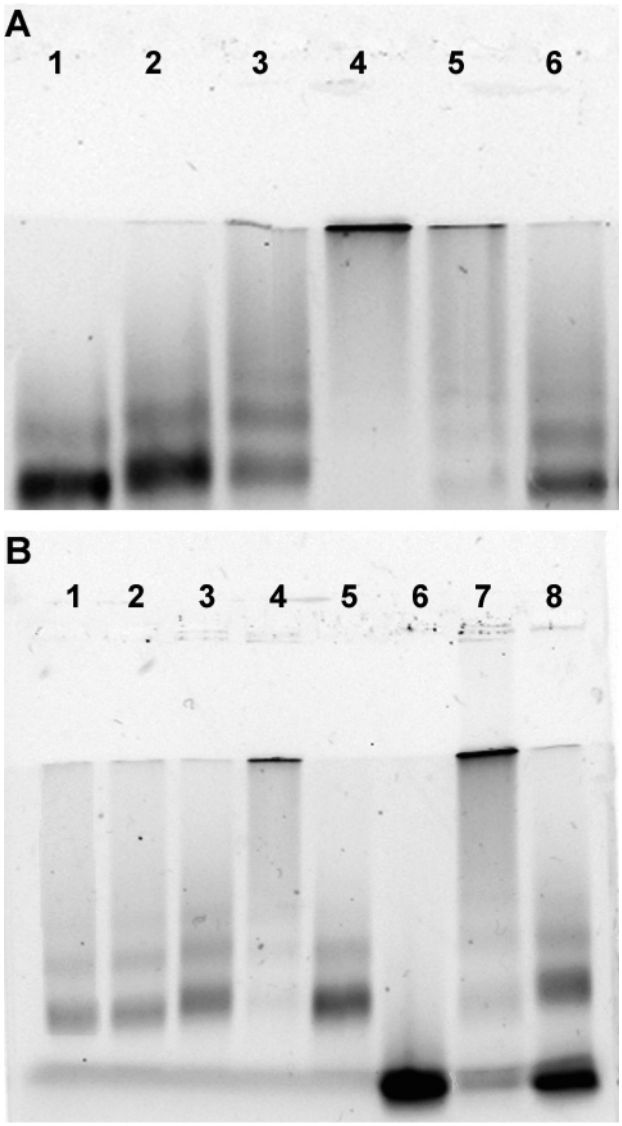

Figure 4. Discontinuous SDS-AGE demonstrated stoichiometry-dependent relative size and molecular weight differences between strep−QDs and QD bioconjugates and confirmed specific biotin−IgG−streptavidin binding. **(**A) There was a modest decrease in the migration of 100:1 (2; 1.25 μM biotin−IgG:12.5 nM strep−QD) and 10:1 (3; 125 nM biotin−IgG:12.5 nM strep−QD) bioconjugate bands compared to strep−QDs (1; 12.5 nM) with a concomitant increase in smearing above the bands. The 1:1 bioconjugates (4; 12.5 nM biotin−IgG:12.5 nM strep−QD) were considerably retarded; the networks did not enter the resolving gel and no bands were visable. At very low biotin−IgG:strep−QD molar ratios (5 and 6; 1.25 nM:12.5 nM strep−QD and 125 pM biotin−IgG:12.5 nM strep−QD, respectively), the QD bioconjugate migration was largely recovered. (B) Strep−QDs (1; 12.5 nM) and biotin−QDs (2; 625 nM biotin:12.5 nM strep−QD) had identical migration patterns. As in panel A, 100:1 bioconjugates (3; 1.25 μM biotin−IgG: 12.5 nM strep−QD) migrated less than strep−QDs but more than 1:1 bioconjugates (4; 12.5 nM biotin−IgG:12.5 nM strep−QD). Incubation of strep−QDs with biotin before introduction of biotin−IgG blocked network formation (5; 12.5 nM strep−QDs:625 nM biotin, followed by 12.5 nM biotin−IgG). The migration of commercial biotinylated QDs (6; 12.5 nM) was retarded considerably when incubated with strep−QDs (7; 12.5 nM strep−QDs:12.5 nM biotinylated QD). The decreased migration in lane 7 was mitigated when biotinylated QDs were added to 100:1 bioconjugates (8; 100:1 bioconjugates from lane 3 and 12.5 nM biotinylated QD).

indicated that there were at least two strep−QD sizes. These commercial strep−QDs are predominantly single particles although dimers and trimers may constitute up to 30% of the total population.[22] Our demonstration of multiple bands in Figure 2 was evidence of this strep−QD population distribution because single strep−QDs constituted the darkest band and strep−QD dimers (and trimers) composed the lighter and heavier bands. The possibility of polydisperse commercial strep−QDs should be considered by researchers who utilize these strep−QDs. Band migration and intensity decreased slightly and smearing above the bands was noted as the biotin−IgG:strep−QD molar ratio decreased (lanes 2−3). Smearing refers to the blurred fluorescence in the gel between the strep−QD bands and the stacking/resolving gel interface. The migration pattern in lanes 2−3 indicated a modest increase in the molecular weights of single QD bioconjugates in addition to the formation of larger, multiple-QD networks. Also, the decrease in strep−QD band intensity was accompanied by an increase in smearing because more QD bioconjugate networks formed as the biotin−IgG:strep−QD molar ratio decreased. The 1:1 QD bioconjugates (lane 4) were significantly retarded at the stacking/resolving gel interface, with no strep−QD bands and some smearing below the interface. This migration pattern suggested a preponderance of very high molecular weight QD bioconjugate networks and a distribution of smaller networks. The presence of very high molecular weight species corroborates the AFM topography (Figure 1) and phase (Figure 2) evidence of large 1:1 bioconjugate networks. QD bioconjugate migration recovered as the biotin−IgG:strep−QD molar ratio was further decreased (lane 5). Bands corresponding to individual QD bioconjugates were faintly discernible in lane 5, and smearing indicated that a range of networks was still present. At a very low biotin−IgG:strep−QD molar ratio (lane 6), strep−QD migration was almost completely recovered and strep−QD bands were clearly visible because there was inadequate biotin−IgG to mediate extensive networking. The multiplicity of several biotins coupled to each IgG probably enabled biotin−IgG molecules to act as bridges between several strep−QDs during formation of QD bioconjugate networks. Network formation caused by the cross-linking of multiple avidin−biotin bridges has been previously observed with peptide-modified QDs[14] and gold nanoparticles.[39] Discontinuous SDS-AGE first established stoichiometry-dependent formation of QD bioconjugates with different relative sizes and molecular weights.

Discontinuous SDS-AGE was then employed to examine specific biotin−IgG:QD binding (Figure 4, panel B). QD biotinylation did not alter strep−QD migration because the size of biotin is negligible compared to the size of strep−QDs (lanes 1 and 2). This result supports our AFM conclusion that strep−QDs and biotin−QDs were of similar size and shape. The migration patterns for 100:1 and 1:1 bioconjugates (lanes 3 and 4) closely matched those in panel A. The decreased migration and smearing of 1:1 bioconjugates was eliminated by blocking strep−QD surface streptavidin sites with excess biotin before biotin−IgG incubation (lane 5), which indicated that the large molecular weight of 1:1 bioconjugate networks was due to biotin−IgG:streptavidin mediated cross-linking of multiple strep−QDs. This streptavidin−biotin mediated networking was also demonstrated in earlier phase AFM images (Figure 2, panels E & F). Commercial biotinylated QDs without surface-conjugated streptavidin molecules migrated further than strep−QDs (lane 6). Streptavidin−biotin mediated cross-linking between biotinlyated QDs and strep−QDs resulted after adding strep−QDs to biotinylated QDs (lane 7). However, when biotinylated QDs were added to 100:1 QD bioconjugates, networks did not form and the biotinylated QD migration was recovered (lane 8). This mobility shift analysis demonstrated specific biotin−IgG modification of 100:1 QD bioconjugates

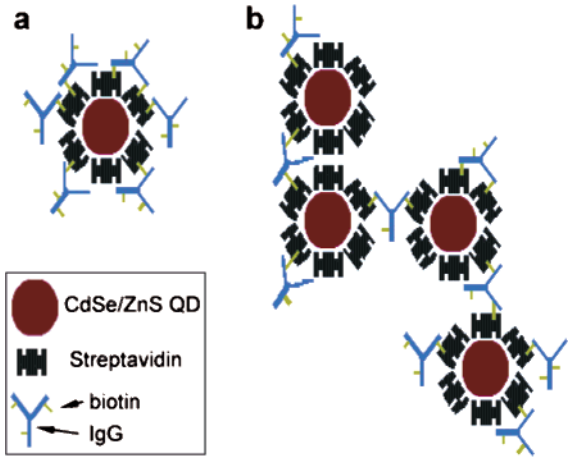

Figure 5. Proposed model of biotin−IgG:strep−QD bioconjugate formation. Black shapes represent streptavidin covalently conjugated to red, circular QDs. IgG molecules are represented as blue Ys, with associated green biotin molecules. At high biotin−IgG:strep−QD ratios (e.g., >10:1, panel a), the biotin−IgG rapidly binds to available sites on streptavidin, essentially coating the strep−QDs. At low biotin−IgG:strep−QD ratios (e.g., 1:1, panel b) there is rapid binding but insufficient biotin−IgG to completely coat the strep−QD surfaces. Each of the 10−15 streptavidin molecules per QD has up to four exposed biotin binding sites. This multivalency and the multiple biotins conjugated to each IgG molecule results in streptavidin−biotin mediated cross-linking between many strep−QDs.

because the biotin binding sites on these QD bioconjugate surfaces were not accessible to biotinylated QDs. Demonstration of successful conjugation in 100:1 QD bioconjugates was significant because AFM analysis did not establish this binding. It is important to note that researchers who utilize streptavidin−biotin chemistry for strep−QD modification and require individual QD bioconjugates without cross-linked networks should employ high biotin−biomolecule:strep−QD molar ratios. SDS-AGE showed stoichiometry-dependent molecular weight and size differences and proved specific biotin−IgG: strep−QD binding in both 100:1 and 1:1 bioconjugates.

Results from AFM height and phase analysis combined with discontinuous SDS-AGE migration patterns are illustrated by a model of QD bioconjugate network formation (Figure 5), which is similar to a gold nanoparticle aggregation model.[39] At high biotin−IgG:strep−QD ratios (panel a), antibodies rapidly bound strep−QD surfaces, essentially coating and blocking all surface biotin-binding sites. The small decrease in migration of 100:1 bioconjugates and the mobility shift analysis illustrated successful biotin−IgG binding to strep−QDs. At lower molar ratios (e.g., 1:1; panel b), there was insufficient biotin−IgG to completely coat the strep−QDs. Therefore, binding sites remained exposed to the multiple biotins on IgG, and large networks formed through streptavidin−biotin mediated cross-linking. The increased size and unique morphology of these networks were easily exhibited with both with AFM and SDS-AGE characterization. Thus, the formation of QD bioconjugates as individually modified particles or multiparticle, cross-linked networks was tightly controlled by the biotin−IgG:strep−QD molar ratio.

Conclusion

Quantitative AFM height data and highly detailed AFM phase images were integrated with high resolution SDS-AGE migration patterns to comprehensively characterize size, morphology and relative molecular weight changes after streptavidin−biotin mediated QD modification. QD bioconjugate assembly was controlled by varying the biotin−IgG:strep−QD stoichiometry, and significant differences among the QD bioconjugates were demonstrated. Specifically, the molar ratio for modification determined whether QD bioconjugate populations consisted of individual modified particles, cross-linked networks or a distribution of both. QD bioconjugates are often used in cellular studies without prior characterization of size or surface modification. QD bioconjugates may possess vastly different sizes, morphologies and molecular weights that will impact cell-QD interaction. The results described above underscore the importance of complete physical characterization of QD bioconjugates with complementary techniques before applying these nanoparticles in biological experiments.

Acknowledgment. The authors thank Dr. Natalia Broude, Dr. Catherine Klapperich, and members of their labs for use of PAGE components. We also thank the B.U. Biology Department for use of the gel documentation system. This work was supported by a Boston University Spring Grant (T.Q.V. and T.A.D.) and EY-13693 from the National Institutes of Health. Partial financial support to B.J.N. was provided by NIGMS Award T32GM008541.

References and Notes

(1) Ozkan, M. *Drug Disc. Today.* **2004**, *9*, 1065−1071.
(2) Jaiswal J. K.; Mattoussi, H.; Mauro, J. M.; Simon, S. M. *Nat. Biotechnol.* **2003**, *21*, 47−51.
(3) Jaiswal, J. K.; Simon, S. M. *Trends Cell. Biol.* **2004**, *14*, 497−504.
(4) Ballou, B.; Lagerholm, B. C.; Ernst, L. A.; Bruschez, M. P.; Waggoner, A. S. *Bioconjugate Chem.* **2004**, *15*, 79−86.
(5) Dahan, M.; Lévi, S.; Luccardini, C.; Rostaing, P.; Riveau, B.; Triller, A. *Science* **2003**, *302*, 442−445.
(6) Chan, W. C. W.; Nie, S. *Science* **1998**, *281*, 2016−2018.
(7) Pathak, S.; Choi, S. K.; Arnheim, N.; Thompson, M. E. *J. Am. Chem. Soc.* **2001**, *123*, 4103−4104.
(8) Gao, X.; Cui, Y.; Levenson, R. M.; Chung, L. W. K.; Nie, S. *Nat. Biotechnol.* **2004**, *22*, 969−976.
(9) Wu, X.; Liu, H.; Liu, J.; Haley, K. N.; Treadway, J. A.; Larson, J, P.; Ge, N.; Peale, F.; Bruchez, M. P. *Nat. Biotechnol.* **2003**, *21*, 41−6.
(10) Nakamura, M.; Tsumoto, K.; Ishimura, K.; Kumagai, I. *Anal. Biochem.* **2002** *304*, 231−235.
(11) Wilchek, M.; Bayer, E. A. *Trends Biochem. Sci*. **1989**, *14*, 408−412.
(12) Wilchek, M.; Bayer, E. A. *Methods Enzymol.* **1990**, *184*.
(13) Wagner, P. *FEBS Lett.* **1998**, *430*, 112−115.
(14) Pinaud, F.; King, D.; Moore, H. P.; Weiss, S. *J. Am. Chem. Soc.* **2004**, *126*, 6115−6123.
(15) Gerion, D.; Pinaud, F.; Williams, S. C.; Parak, W. J.; Zanchet, D.; Weiss, S.; Alivisatos, A. P. *J. Phys. Chem. B* **2001**, *105*, 8861−8871.
(16) Nagao, E.; Dvorak, J. A. *Biophys. J.* **1999**, *76*, 3289−3297.
(17) Raghavan D.; Gu, X.; Nguyen, T.; VanLandingham, M.; Karim, A. *Macromolecules* **2000**, *33*, 2573−2583.
(18) Tamayo, J.; Garcia, R. *Langmuir* **1996**, *12*, 4430−4435.
(19) Viswanathan, R.; Tian, J. *Langmuir* **1997**, *13*, 1840−1843.
(20) Vu, T. Q.; Maddipati, R; Blute, T. A.; Nehilla, B. J.; Nusblat, L.; Desai, T. A. *Nano Lett.* **2005**, *5*, 603−607.
(21) Pris, A. D.; Porter, M. D. *Langmuir* **2004**, *20*, 6969−6973.
(22) Quantum Dot Corp., personal communication with technical support staff.
(23) Zanchet, D.; Michael, C. M.; Parak, W. J.; Gerion, D.; Williams, S. C.; Alivisatos, A. P. *J. Phys. Chem. B* **2002**, *106*, 11758−11763.
(24) Zanchet, D.; Michael, C. M.; Parak, W. J.; Gerion, D.; Alivisatos, A. P. *Nano Lett.* **2001**, *1*, 32−35.
(25) Sandstrom, P.; Akerman, B. *Langmuir* **2004**, *20*, 4182−4186.
(26) Nikiforov, T. *Quantum Dot Vision* **2004** *January* 12−14.
(27) Parak, W. J.; Gerion, D.; Zanchet, D.; Woerz, A. S.; Pellegrino, T.; Micheel, C.; Williams, S. C.; Seitz, M.; Bruehl, R. E.; Bryant, Z.; Bustamante, C.; Bertozzi, C. M.; Alivisatos, A. P. *Chem. Mater.* **2002**, *14*, 2113−2119.
(28) Ebenstein, Y.; Mokari, T.; Banin, U. *J. Phys. Chem. B* **2004**, *108*, 93−99.
(29) Nehilla, B. J.; Popat, K. C.; Vu, T. Q.; Chowdhury, S.; Standaert, R. F.; Pepperberg, D. R.; Desai, T. A. *Biotechnol. Bioeng.* **2004**, *87*, 669−674.

(30) Ebenstein, Y.; Nahum, E.; Banin, U. *Nano Lett.* **2002**, *2*, 945−950.
(31) Bergkvist, M.; Carlsson, J.; Karlsson, T.; Oscarsson, S. *J. Colloid Interface Sci.* **1998**, *206*, 475−481.
(32) Ouerghi, O.; Touhami, A.; Othmane, A.; Ouada, H. B.; Martelet, C.; Fretigny, C.; Jaffrezic-Renault, N. *Sens. Actuators, B* **2002**, *84*, 167−175.
(33) Schneider, S. W.; Larmer, J.; Henderson, R. M.; Oberleither, H. *Eur. J. Physiol.* **1998**, *435*, 362−367.
(34) Tang, Z.; Wang, Y.; Kotov, N. A. *Langmuir* **2002**, *18*, 7035−7040.
(35) Laemmli, U.K. *Nature* **1970**, *227*, 680−685.
(36) Raines, G.; Aumann, H.; Sykes, S.; Street, A. *Thrombosis Res.* **1990**, *60*, 201−212.
(37) Deutscher, M. P. *Methods Enzymol.* **1990** *182*.
(38) Quantum Dot Corp. *Qdot Streptavidin Conjugates User Manual*, rev 9.2. www.qdots.com.
(39) Aslan, K.; Luhrs, C. C.; Perez-Luna, V. H. *J. Phys. Chem. B* **2004**, *108*, 15631−15639.